Laser Surface Alloying of Aluminum on Iron Substrate: Experiments and Numerical Simulation

G. Phanikumar, B.Basu, S. Chakraborty, K. Chattopadhyay, P. Dutta and J.Majumder[+]
Indian Institute of Science, Bangalore 560012, India
[+]University of Michigan, Ann Arbor, MI 48109-2125, USA

1 Introduction

Laser surface alloying allows synthesis of intermetallic coatings and compositional gradient materials on the surface for better surface properties. The process typically consists of a moving laser beam with a constant scanning speed in the horizontal direction over a substrate, a thin layer of which melts and forms a pool due to laser heating. Simultaneously, a powder of a different material is fed into the pool, which then mixes with the molten substrate by convection and diffusion. As the laser surface moves away from a location where the pool is already developed, resolidification of the zone occurs leading to a final microstructure of the alloyed surface.

An objective of research in this area is to study microstructure evolution, phase formation and their effect on the properties of the alloyed region as a function of process parameters such as powder feed rate, laser scan speed and heat input [1-3]. The physical processes that take place in the laser molten pool and subsequent solidification are complex, rendering a functional relation between the process parameters and the properties of the alloyed region, a difficult task. In the present study, we attempt to understand microstructural development during laser surface alloying of aluminum on iron substrate. We also make an attempt to mathematically model and computationally simulate the transport phenomena involved in the process, in order to predict the pool shape and size, heat and fluid flow, and final composition distribution in the resolidified zone.

2 Experimental Work

The surface alloying was done using a 5 kW cw-CO_2 laser (Trumf make) operated at a peak power of 4.3 kW. A beam diameter of 2mm was used for all experiments. The aluminum powder was fed in the melt pool using a gravity powder feeder with helium as the carrier gas. Composition of the substrate (wt%) is 0.024 C + 0.004 Si + 0.048 Mn +

0.012 S + 0.006 P + 0.001 Cr + 0.003 Ni + 0.001 Mo. The powder feed rate was varied from 0.02 to 0.115 gs^{-1} and traverse speed of the substrate was varied from 0.003 to 0.017 ms^{-1}. XRD, SEM, EDAX and micro-hardness were used to characterize the alloyed regions. We discuss results of the processing conditions for which microstructural transitions are most distinct.

Figure 1 gives XRD patterns for an alloyed surface with a powder feed rate of 0.02 gs^{-1} for the cases of maximum (0.017 ms^{-1}) and minimum (0.003 ms^{-1}) traverse speeds. It is observed that when the traverse speed is increases, formation of γ– and α-Al_2O_3 and Fe_3Al decreases. The lower traverse speed of laser results in the appearance of peaks of γ and α Al_2O_3 in addition to the peaks corresponding to Fe-Al bcc solid solution. The intensity of the oxide peak decreases with the increasing traverse speed. At the highest scan rate, XRD patterns do not show the existence of peaks corresponding to the Al_2O_3 phases for any powder feed rate, indicating that higher interaction time promotes oxide formation of the powder.

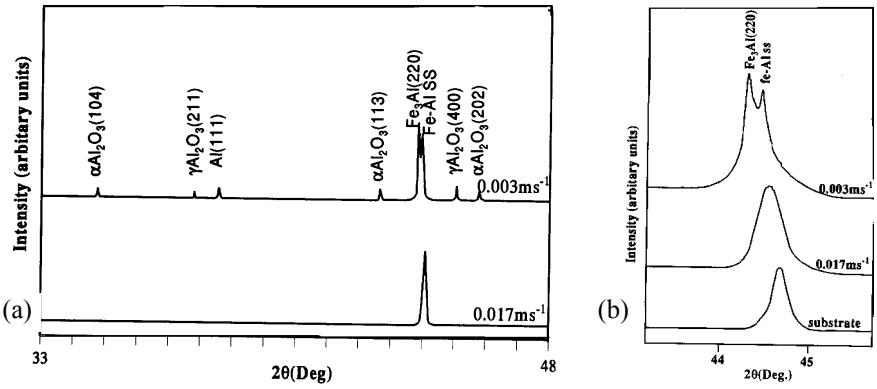

Figure 1 (a). XRD patterns for laser alloyed samples for constant Al feed rate of 0.02 gs^{-1} and traverse rates of 0.003 and 0.017 ms^{-1} (b) Evolution of (110) peak. The corresponding peak from the substrate is also shown.

A typical microstructure of alloyed region is shown in figure 2a. Microstructural features change from the substrate towards the top of the alloyed region. The uniform coarse grains of substrate are first followed by a fine-grained microstructure and then by a columnar grain structure extending to the top of the surface. The column grows perpendicular to the melt/substrate interface towards the center of the laser molten pool. The bending of the columnar grains towards maximum thermal gradient is clear from the longitudinal section in figure 2b. The amount of the columnar and equiaxed zones in a given sample depends on the process variables. There exists a very dramatic change in the microstructure form as the traverse speed is increased.

Microstructures of the laser alloyed regions for the cases of two extreme traverse speeds and with a feed rate of 0.02 gs^{-1} are shown in figure 3. For a low traverse rate ($0.003ms^{-1}$), the samples show a dominant zone of columnar microstructure (fig.3a). No columnar zone could be seen for a high traverse rate of $0.017ms^{-1}$ (fig3b). The laser molten pool in this case essentially consists of fine grains.

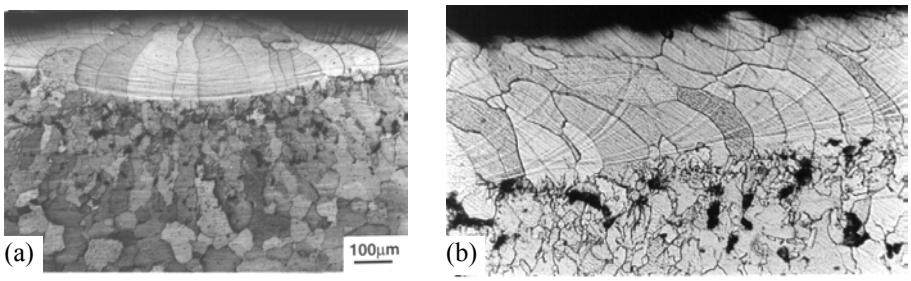

Figure 2. Representative Microstructures of transverse cross-section of laser alloyed samples showing three distinct zones (feed rate of $0.04gs^{-1}$ and traverse rate of substrate $0.008ms^{-1}$)

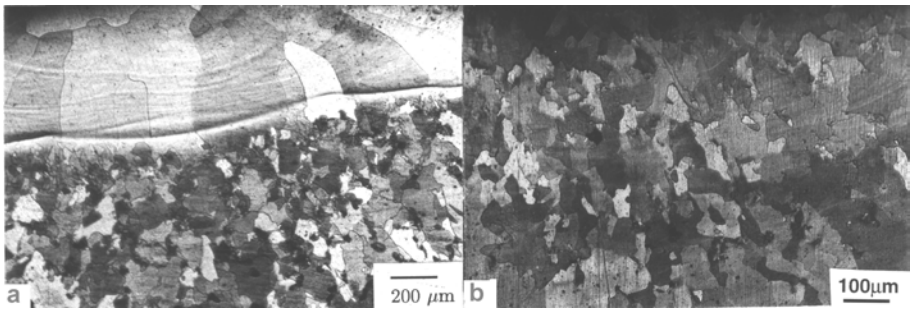

Figure 3. Comparative micrograph of transverse-section of laser alloyed region for a feed rate of $0.02gs^{-1}$ under two extreme traverse rates: (a) $0.003ms^{-1}$ and (b)$0.017ms^{-1}$.

The micro-hardness profiles of the transverse section of the laser molten pool corresponding to the above two cases are shown in figure 4. The hardness profile increases sharply near the surface in both the cases. The hardness value reaches a maximum of 390VHN for the case of low traverse rate. This corresponds to the reported hardness value of ordered Fe_3Al [4]. For the sample processed with high laser traverse rate the maximum hardness is much smaller (~220VHN) indicating the formation of solid solution grains. However, these samples show a small but distinct hardness gradient in the substrate below the laser melted zone.

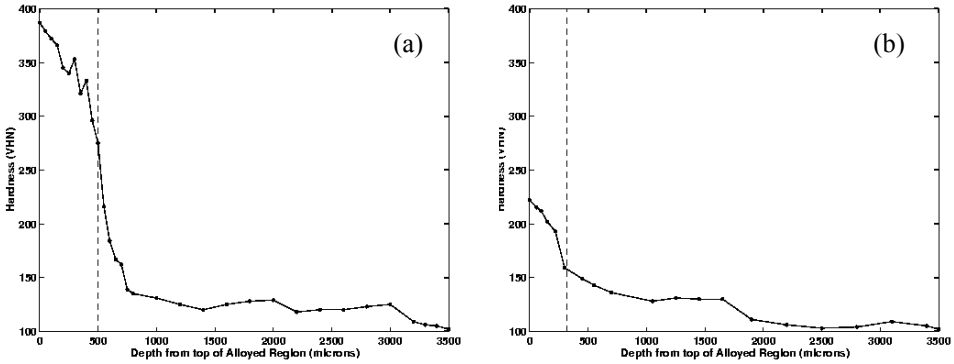

Figure 4. Microhardness profile along the depth of laser alloyed pool at Al feed rate of 0.02gs^{-1} under traverse rates of (a)0.003ms^{-1} and (b)0.017ms^{-1}.

3 Numerical Simulation

Since this is a moving heat source problem, laser surface alloying is best studied in a coordinate frame that is fixed to the laser source. In such a case, the governing differential equations have to be modified according to an appropriate transformation law, leading to the creation of additional term(s) in the transformed governing equation. If ϕ is a general scalar variable for which we write a governing differential equation arising out of a conservation law, the general convection-diffusion equation in the transformed frame is as follows:

$$\frac{\partial}{\partial \mathrm{t}}(\rho\phi) + \nabla \cdot (\rho \vec{u}\phi) = \nabla \cdot (\Gamma \nabla \phi) + S + S_{transform} \tag{1}$$

where, ρ is the density of the medium, $\vec{u}$ is the velocity, Γ and S are the diffusivity and the source term, respectively, of the corresponding ϕ, and $S_{transform}$ is the additional source term arising out of coordinate transformation. Substituting for the appropriate ϕ in equation 1, we can write equations for the conservation of mass, momentum, energy and species. Phase change is modeled using an enthalpy-porosity approach [5]. All governing equations are three-dimensional, due to the nature of the laser surface alloying problem. Detailed governing equations and boundary conditions for the momentum and energy conservation equations are available in [6], and have been omitted here for the purpose of brevity. For the species conservation equation, the boundary conditions are as follows:

Top surface (under the laser): $-D\frac{\partial C}{\partial y} = \dot{q}$ (2)

Fusion front: $(1-k)vC = -D\frac{\partial C}{\partial x}$ (3)

Solidification front: $vC = -D\frac{\partial C}{\partial x}$ (4)

In the above expressions, D is the mass diffusivity, C is the concentration, v is the velocity of the front along laser scan (x) direction and k is the partition coefficient.

(a)

(b)

(c)

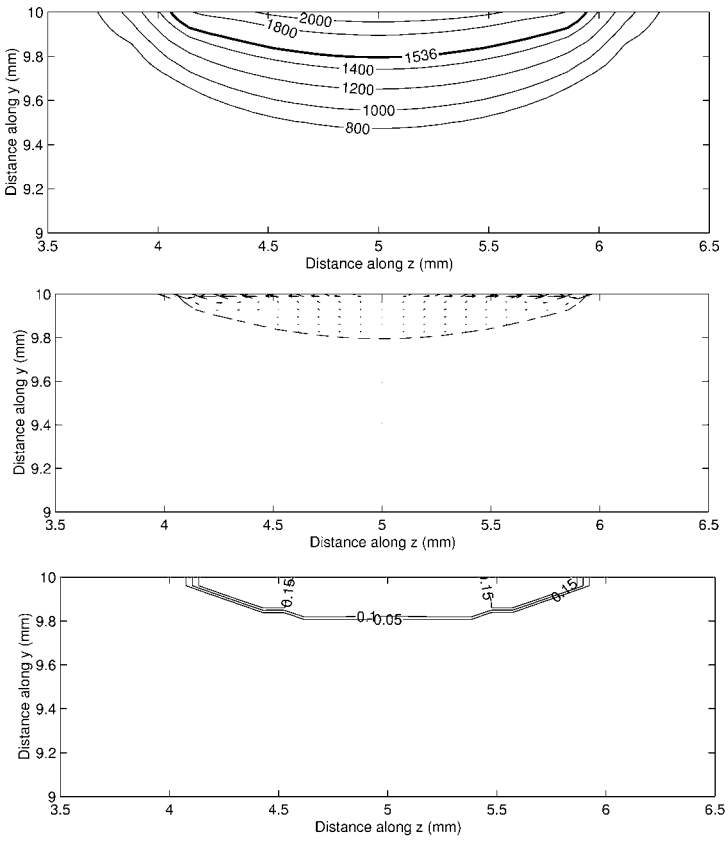

Figure 5. Calculated (a) temperature contours (b) velocity profile and (c) composition contours for a traverse speed of 0.017 ms^{-1} and a powder feed rate of 0.02gs^{-1} (transverse section)

We have carried out numerical simulation for several traverse speeds and feed rates. A typical numerical result is shown in figure 5, which depicts the calculated temperature,

velocity and composition distributions with a traverse speed of $0.017ms^{-1}$ and feed rate of $0.02\ gs^{-1}$. The alloyed pool shape, size and composition distribution show a good qualitative agreement with the corresponding experimental results. The calculated composition gradient at the bottom of the pool is sharp, as observed indirectly by the micro-hardness profile (fig. 4b) that shows solid solution strengthening at the bottom of the alloy pool. However, the aspect ratio of the computed alloyed pool is slightly larger than the corresponding experimental one. We attribute this difference to the uncertainty of some of the inputs (such as laser coupling efficiency, surface tension coefficient, etc.) to our computational model.

4 Conclusions

Microstructure evolution during laser surface alloying of iron with aluminum has been studied. The microstructure and hardness of the alloyed region are dependent on the laser scan rate. The results suggest that the fine grains observed near the substrate are of solid solution of Al in Fe. For the samples with low traverse speed, the lattice parameter and the hardness profile confirm that the intermetallic Fe_3Al forms near the surface. A composition of 17 at% Al is obtained by the EDAX near the top surface of the columnar grain, which further supports this conclusion since this composition enters into Fe_3Al phase field. For samples with high scan rate, the microstructure changes over to a columnar structure near the top.

A numerical simulation of the process is able to predict the shape and size of the pool along with temperature, velocity and composition distributions. Some of the trends suggest a good qualitative agreement with the experimental results.

5 References

1. T. Chande and J. Mazumder, Appl. Phys. Lett., 1982, 41, 42.
2. I. Manna, J. D. Majumdar, U. K. Chatterjee & A. K. Nath, Scr. Mater.,1996, 35, 405.
3. X. He, B. Mordike, N. Pirch and W. Kreutz, Lasers in Engineering, 1995, 4, 291.
4. Bahadur, O. N. Mohanty, J. Mater. Sci., 1991, 26, 2685.
5. D. Brent, V. R. Voller, and K. J. Reid, Numerical Heat Transfer, 1988, vol. 13, 297-318.
6. P. Dutta, Y. Joshi, and R. Janaswamy, Numerical Heat Transfer A, 1995, 27, 499 - 518.